Applied Thermal Engineering 59 (2013) 162–173

Contents lists available at SciVerse ScienceDirect

Applied Thermal Engineering

journal homepage: www.elsevier.com/locate/apthermeng

Study of an exhaust gas recirculation equipped micro gas turbine supplied with bio-fuels

Maria Cristina Cameretti [a], Raffaele Tuccillo [a,*], Renzo Piazzesi [b]

[a] Dipartimento di Ingegneria Industriale (D.I.I.), Università di Napoli Federico II, Via Claudio 21, 80125 Napoli, Italy
[b] ANSYS UK Ltd., Abingdon, UK

HIGHLIGHTS

- External and internal EGR concepts applied to NOx control from micro gas turbines.
- For gaseous fuels: internal EGR is obtained by a proper location of the pilot injector.
- For liquid fuels: replacing the original radial injectors with a pressure swirl atomizer.
- We apply a CFD based method, after validation with experimental data.
- Blends of bio-fuels with fossil fuels promise noticeable benefits.

ARTICLE INFO

Article history:
Received 5 December 2012
Accepted 15 April 2013
Available online 27 May 2013

Keywords:
Micro gas turbine
Bio-fuels
Mild combustion
CFD

ABSTRACT

The authors discuss in this paper some aspects related to the employment of liquid and gaseous bio-fuels in a micro-gas turbine. Besides the purpose of checking the effectiveness of methods for supplying the micro-turbine with fuels from renewable sources, the attention is focused on the need of controlling the pollutant emission. To this aim, several solutions are experienced and numerically tested. For the liquid fuel supply, a new shape and location of the main fuel injector is combined with a modified position of the pilot injector. In the case of the biogas fuelling, an external EGR option is considered as activated. Both methods aim at the reduction of the thermal and prompt NO formation by approaching the flameless combustion concept.

1. Introduction

In their recent papers [1–6], the authors have developed a comprehensive investigation of several aspects concerning the flameless concept for reduced nitric oxide emissions from micro gas turbines. The flameless combustion has been studied experimentally and/or numerically by several authors in different combustion systems [7–10] to individuate the best conditions lead to higher temperature uniformity. As well known, activating an exhaust recirculation [11–13] to the compressor inlet allows the combustion chamber to be addressed by an air-gas mixture with a relevant oxygen defect. Such a condition, together with the high temperature level induced by the recuperated cycles, leads the combustion development to situations close to the so-called MILD regime. These papers have first highlighted the advantages that arise from the adoption of an external EGR system, together a number of limitations, say:

- A performance decay that derives from the decreased compressor flow capacity and pressure ratio, because of the exhaust-air mixing.
- The increase in carbon monoxide and unburned species emissions that result from the smoother combustion regime.

In their most recent papers [4–6] the authors have demonstrated that the above problems may be partly overcome by simple, low-cost, modifications to the combustor assembly, like a different location of the pilot injector. This solution, once the optimal location has been determined, allows activation of the reactant ignition in a zone with a relevant presence of inert species, so inhibiting the thermal NOx formation.

Both solutions are of particular interest at part load operation of the micro gas turbine, because of the increased fuel flow rate that is addressed to the pilot line. In some cases, the combined employment of the modified pilot location with a limited EGR rate allows to approach emission free combustion regimes when supplying the chamber with natural gas or kerosene.

* Corresponding author. Tel.: +39 (0)817683302; fax: +39 (0)812394165.
E-mail address: tuccillo@unina.it (R. Tuccillo).

1359-4311/$ – see front matter © 2013 Elsevier Ltd. All rights reserved.
http://dx.doi.org/10.1016/j.applthermaleng.2013.04.029

Nomenclature

CHP	combined heat and power plant
EGR	exhaust gas recirculation
f	fuel/air ratio
LPP	lean-premixed prevaporized
$\dot{m}$	mass flow rate, [kg/s]
MGT	micro gas turbine
OFR	oxygen/fuel ratio
p	pressure, [bar]
p.p.m.	parts per million (on wet basis)
p.p.m.d.	parts per million (on dry basis)
R	reaction rate, [kmole/(m^{3}s)]
T	temperature [K]
T_{of}	standard adiabatic flame temperature [K]
X_b	recuperator by-pass ratio
X_{egr}	EGR ratio

Subscripts

a	air
ex	combustion chamber exit
f	fuel
in	combustion chamber inlet
g	exhaust gas
cc	mixing conditions
ox	oxidant
st	stoichiometric
R	recuperator

Basing on the above encouraging experiences, the authors examine in this paper the off-design conditions that are induced in the combustor by non-conventional fuels, like those pertaining to the biogases or bio-diesel category. Actually, the different fuel composition and the changes in fuel/air ratios that are needed for reaching the rated conditions of the micro-turbine can induce an off-design behaviour of the combustor and, consequently, an increase in NOx emission. In this sense the same analysis as the one carried out for conventional fuels is worthy of refinement in order to get validation from a wider range of fuelling conditions.

The numerical techniques combine a matching analysis of the whole system with a CFD simulation of the combustor and both natural gas and gaseous bio-fuels are considered. The aim is to find the optimal combination of the EGR rates and pilot injector location for minimizing the emissions in a wide range of the micro gas turbine operation.

The authors pay special attention to the challenging problem of the employment of renewable energy sources in distributed energy system: actually, a particular care must be addressed to a satisfactory compromise between the expected CO_2 reduction and possible increases in pollutant emissions, like carbon and nitric monoxides. Under this stringent aspect, examples refer to both gaseous and liquid bio-fuels. The latter case involves particular attention to be paid to the choice of the injection system, that should also ensure an effective droplet atomization and, more generally, a satisfactory mixture preparation process [6,14]. To this purpose, different low-cost solutions are examined for the shape and location of the fuel nozzles.

2. External EGR concept

Like recalled above, a number of authors' papers [1–6] provide a detailed description of the modified layout of the 110 kW micro-gas turbine, based on the introduction of an exhaust recirculation (EGR) circuit (Fig. 1). The recuperator by-pass option allows adaptation of the MGT output to different electrical and thermal power demands. This feature, together with the variable speed operation, allows a noticeable flexibility of a MGT based CHP system. If looking at constant speed operation with fully recuperated cycles, the MGT response is chiefly governed by the EGR ratio:

$$X_{egr} = \frac{\dot{m}_{egr}}{(1 - X_b)\dot{m}_g} \tag{1}$$

Increasing the above parameter allows achievement of combustion regimes close to those recognizable as *MILD* or *flameless* ones. Actually, the oxygen defect in the oxidant together with the high combustor entry temperature that results from the recuperated cycles generate conditions that allow a fair approximation of the MILD combustion regime [1,15] with much smoother temperature profiles and reduced nitric oxide formation rates.

Referring to examples that are of interest in this paper, a comprehensive overview of the EGR effects is provided by the diagrams in Figs. 2–6. The first examples regard gaseous fuels, and they are addressed to the comparison of the MGT performance and emissions with natural gas of biogas fuelling. The latter presents a typical composition (Table 1) that results from an anaerobic digestion treatment of bio-masses or organic wastes [16]. In Table 2 the expected MGT performance are reported together with a preliminary estimate of the thermal nitric oxide production at full load. Basing on these results, it could be concluded that the biogas fuelling preserves the mechanical output and efficiency levels, while it exhibits a more favourable behaviour in terms of pollutant emissions. Such indications are worthy of validation by a CFD based approach, since they result from a thermo-kinetic model [1–6] that is sensitive to overall parameters, like the adiabatic flame temperature (Table 1), the fuel and oxidant compositions and the air-fuel rates splitting into the different combustor regions.

The curves in Figs. 2–4 describe the effect of the exhaust recirculation. In particular, Fig. 2 puts into evidence that the benefits in terms of NO reduction are counterbalanced by an efficiency decrease. The latter can be explained by a decay in the thermodynamic conversion process that results from both the increased temperature level at the compressor inlet (in despite of the after cooling of the mixed species) and the decreased heat recovery effectiveness in the recuperator. The latter effect is confirmed in Fig. 3, if looking at the decrease in combustor entry temperature when the EGR ratio increases. The higher values of this temperature (by nearly 6–10 K), which can be observed for biogas fuelling, can be explained by the increased exhaust flow rate through the

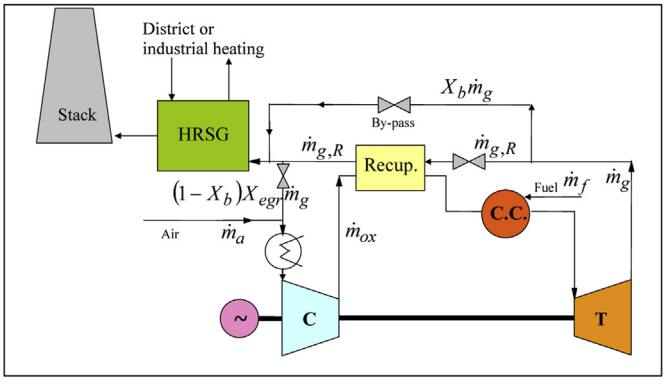

Fig. 1. Plant layout of the recuperated micro-gas turbine with the exhaust recirculation option.

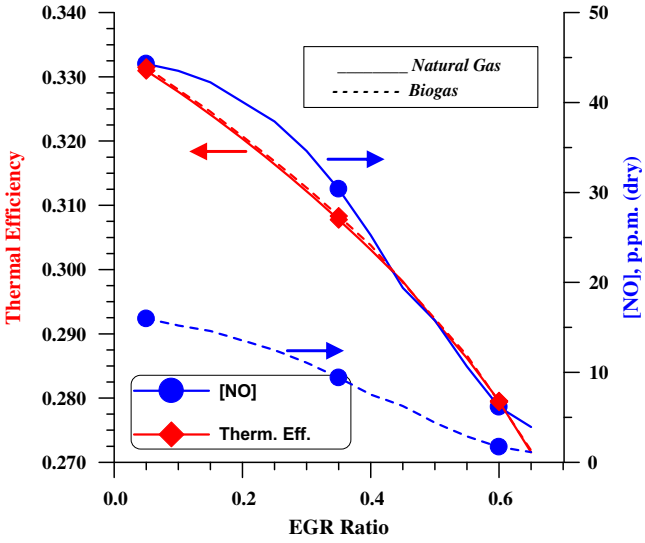

Fig. 2. The EGR effect on MGT efficiency and emissions (full load, fully recuperated cycles).

recuperator. In the same Fig. 3, the much stronger decrease in the combustion peak temperature can be intended as the main reason for the reduction in the nitric oxide formation rate and it can be strictly related with the variations in the oxidant composition that are displayed in Fig. 4. Under the several aspects discussed above, the biogas presents a more favourable behaviour because of its initial contents in inert species.

Similar considerations can be drawn if considering liquid fuels [17–19], like a conventional kerosene and a bio-ethanol, whose properties (Table 3) are approximated by those of the ethylic alcohol [6]. The bio-ethanol fuelling could lead to a slight increase in thermal efficiency but, under the point of view of the NO emission, it appears to be less favourable than the biogas. Therefore, the adoption of the EGR options could be more appropriate in this case and, more generally, when a liquid fuel supply is considered for the micro-gas turbine. Actually, the diagrams in Figs. 5 and 6 present a trend similar to those referring to the gaseous fuels in Figs. 2 and 3, but the nitric oxide levels are higher. This would imply increased EGR rates to meet more acceptable emission limits.

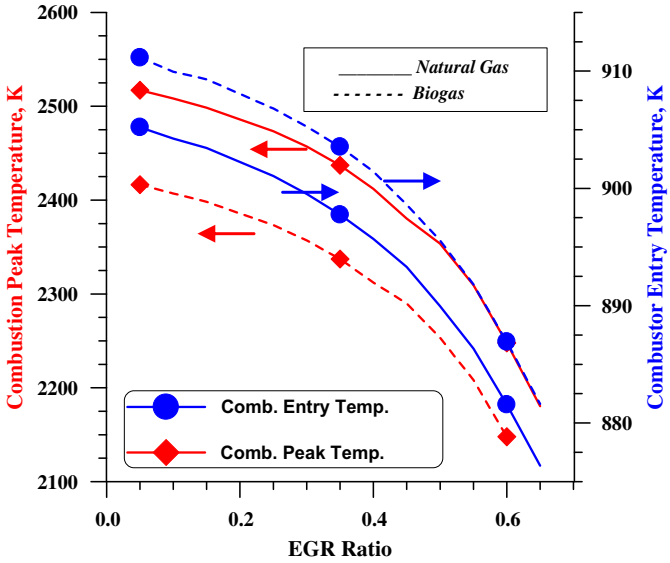

Fig. 3. The EGR effect on the combustion temperatures.

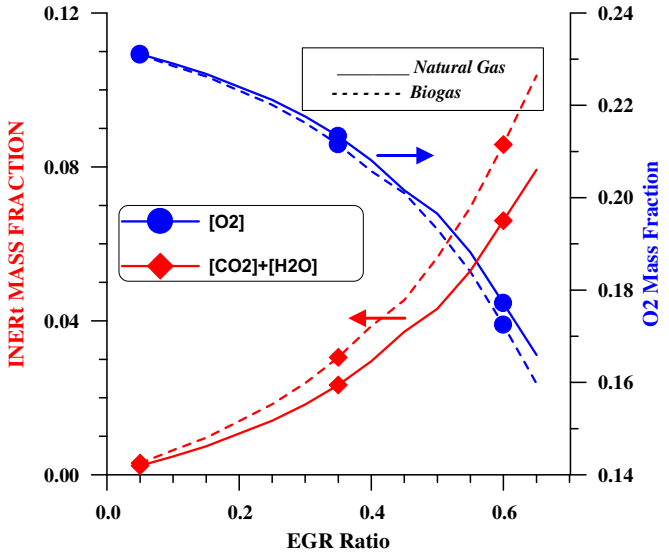

Fig. 4. The EGR effect on the oxidant composition.

Some key aspects of the external EGR option can be finally underlined:

- The external EGR allows the zero NOx emissions to be approached only if the recirculation ratio X_{egr} is greater than 0.6, so leading to a non-negligible performance decay of the micro-gas turbine.
- For natural gas fuelling, the benefits are more evident at part-load [1–4], as a direct consequence of the lean-premixed operation that requires increased fuel rates to the pilot line when the overall equivalence ratio is reduced. In the case of liquid fuels, noticeable advantages appear to be achievable also at full load (Fig. 2).
- The ethanol composition, which is approximated by the bio-fuel examined, seems to be more favourable of kerosene both in terms of thermal efficiency and thermal NO reduction (Fig. 2).

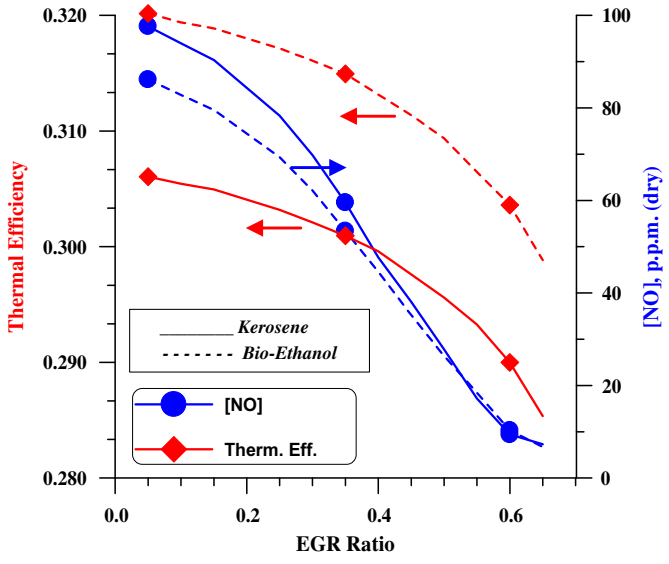

Fig. 5. The EGR effect on MGT efficiency and emissions (full load, fully recuperated cycles).

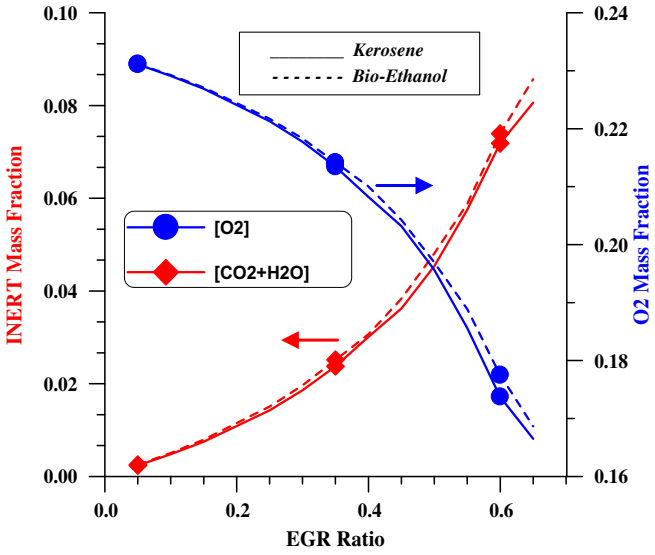

Fig. 6. The EGR effect on the oxidant composition.

It should be underlined that the results in Tables 2 and 4 and the curves in Figs. 2–6 are obtained by a detailed matching model that was setup and experimentally validated by the authors in recent years [1]. The model includes the thermal NO prediction, via a thermo-kinetic approach. Once achieved this first assessment of the main response of the micro-gas turbine to the biofuel supply, a deeper insight on the main phenomena that govern the combustion development and pollutant formation is needed.

3. Internal EGR option and modified injector locations

3.1. The internal EGR

The previous authors' papers [4–6] have demonstrated that, at least at full load operation, the external EGR option in Fig. 1 may be successfully replaced by a simpler, more efficient solution that founds on a different location of the pilot injector within the LP or LPP combustor. Such a solutions exploits the typical vortex pattern (Fig. 7) in the primary region that results in an internal recirculation of the combustion gases. In this way, the pilot injector takes place in a region with poor oxygen and high inert contents and this reduces the temperature peaks and, consequently the NO formation rates. The practical solution consists in a different location of the pilot injector, like evidenced by Figs. 8 and 9 and the benefits from this choice are widely discussed in the referenced authors' papers, which demonstrate that the flameless regime may be successfully approached.

In addition to the modified pilot location, in the case of the liquid fuel supply the authors have considered the possibility of adopting a widely diffused commercial injector, of the Delavan type with a fairly realizable location at the external wall of the premixing channel, just downstream of the air swirling blades. Such an injector has been analysed by the authors in a number of papers [20], and its behaviour is predictable by a good availability of experimental and numerical data. Details of the injector location and its geometry are given in Fig. 10.

The above solution could be of practical interest since it represents a low-cost, well consolidated option that would allow an efficient liquid fuelling and would preserve, at the same time, the radial injectors for a gaseous fuel operation.

Before proceeding with the complete combustion process simulation, a preliminary analysis was needed as to check the effectiveness of the swirling injector that is usually employed in larger size lean-premixed combustors, when adapted to this particular application. As an example, Fig. 11 shows the progress in the atomization process and in the air-fuel mixing in the LPP channel. Following an approach already experienced by the authors in previous works [20], the droplet motion at the nozzle exit is directly generated by the liquid flow throughout the swirling channels of the injector (Figs. 10 and 11).

Since the Delavan nozzle generates a swirled hollow cone spray, the injection pattern may be approximated with reduced computational cost by the hollow cone model already implemented in the flow solver. The model setup utilizes the indications provided by the above more accurate liquid flow and droplet motions

Table 1
Natural gas and biogas properties.

Fuel composition (%, molar)	Natural gas	Biogas
CH_4	92.00	65.00
C_2H_6	3.70	–
C_3H_8	1.00	–
C_4H_{10}	0.25	–
N_2	2.90	–
CO	–	–
CO_2	0.15	35.00
Mol. mass, g/mol	17.34	25.83
ρ, kg/Stdm^3	0.733	1.092
LHV, kJ/kg	47,182	20,183
LHV, kJ/Stdm^3	34,590	22,047
f_{st}	0.0620	0.145
α_{st}	16.13	6.91
T_{of}, K	2220	2126

Table 2
Comparison of MGT performance with natural gas and biogas fuelling.

	Natural gas	Biogas
Base rating, fully recuperated cycle (Xb = 0)		
Mechanical output	109.7	110.4
Thermal efficiency	0.334	0.335
Pressure ratio	3.84	3.84
Compressor exit temp.	468 K	468 K
Turbine inlet temp.	1223 K	1223 K
Turbine exit temp.	952 K	953 K
Recuperator exit temp.	530 K	531 K
Combustor inlet temp.	906 K	912 K
Oxidant mass flow rate	0.808 kg/s	0.808 kg/s
Fuel mass flow rate	0.00695 kg/s	0.01635 kg/s
Fuel % to pilot	10%	10%
Overall equiv. ratio	0.139	0.139
LPP line equiv. ratio	0.452	0.452
Pilot line equiv. ratio	1.000	1.000
Expected thermal NO	42 p.p.m.d.	16 p.p.m.d.

Table 3
Kerosene and ethanol data employed for the MGT performance and combustion simulation.

	Kerosene	Ethanol
LHV, kJ/kg	43,124	27,500
F_{st}	0.0685	0.0957
(OFR) st	3.401	2.435
Dynamic viscosity, kg/(ms)	0.0024	0.0012
Surface tension, N/m	0.0263	0.0223
Vaporiz. temp. (1.013 bar), K	271	341

Table 4
Comparison of MGT performance with kerosene and bio-ethanol fuelling.

	Kerosene	Ethanol
Base rating, fully recuperated cycle (Xb = 0)		
Mechanical output	110.4	111.5
Thermal efficiency	0.339	0.353
Pressure ratio	3.84	3.84
Compressor exit temp.	468	468
Turbine inlet temp.	1223	1223
Turbine exit temp.	952	952
Recuperator exit temp.	530	530
Combustor inlet temp.	905 K	905 K
Oxidant mass flow rate	0.808 kg/s	0.808 kg/s
Fuel mass flow rate	0.00756 kg/s	0.0115 kg/s
Fuel % to pilot	10%	10%
Overall equiv. ratio	0.137	0.148
LPP line equiv. ratio	0.445	0.484
Pilot line equiv. ratio	0.920	1.280
Expected thermal NO	66 p.p.m.d	57.2 p.p.m.d

computation, in terms of cone angle and thickness and droplet average velocity and diameter. The simplified approach allowed a preliminary analysis of additional features of the spray. In particular, Figs. 12 and 13 compare the droplet diameter and fuel vapour distribution, respectively, for different injection conditions, say:

(a) 0° cone axis; positive swirl
(b) −45° cone axis; positive swirl
(c) 0° cone axis; negative swirl

The axis slope is evaluated with respect to the combustor axis, while the swirl orientation refers to the main swirled air motion that is induced by the bladed vanes upstream of the premixing channel.

The different cone assets produce significant variations in both the droplet atomization and in the lean-premixing process, so that such numerical experiments are helpful for determining the optimal conditions to be imposed to the complete CFD combustion simulations, like described in the following section.

4. The CFD analysis of the combustor

4.1. Liquid fuel supply

The cases with the liquid fuel supply aim at the comparison of the combustion development and pollutant formation induced by a conventional fuel like the kerosene and a product of renewable sources like the bio-ethanol [21–25]. As well known, the bio-ethanol represents a widely diffused component in liquid fuel mixtures obtained by the biomass treatment [22]. In Ref. [23] several blends have been tested and the results suggest that an optimum mixture may be found that reduces NOx and CO emissions while producing the desired performance. In Ref. [24] the authors compare theoretically the NO*x* emission tendency of the different bio-fuels of interest in industrial condition, of the conventional petroleum-based fuels, and of natural gas used as a baseline. They considered the adiabatic flame temperature the major determinant of NO*x* emissions in a gas turbine and it has been taken as the criterion. In the present work, the pure ethanol fuelling is considered in order to establish a baseline level of comparison with the employment of conventional fuels. The additional possibility of supplying the main LPP line with bio-ethanol and the pilot injector with kerosene was already considered in paper [6] and it is of interest especially at part-load or during the start-up and shutdown of the micro-gas turbine.

The main properties of the liquid fuels are summarized in Table 3, which also puts into evidence the main parameters that affect the fundamental processes, like the droplet atomization and the reactant mixture quality in the different regions of the chamber. The air and fuel flow rate data refer to the base rating operation that implies a firing temperature of nearly 1220 K at 3.8 bar.

The numerical simulation setup for the analysis of the flow and thermochemical processes inside the tubular combustor of the micro-turbine relies on the following aspects:

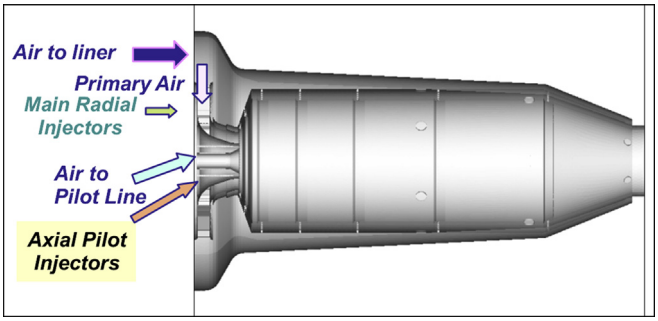

Fig. 8. The lean-premixed combustor.

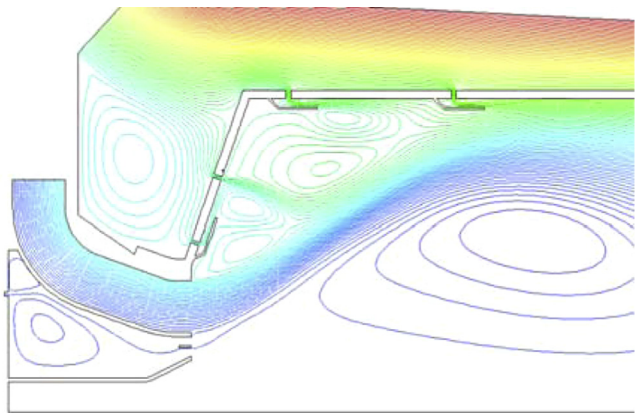

Fig. 7. Streamlines and vortex pattern in the primary region.

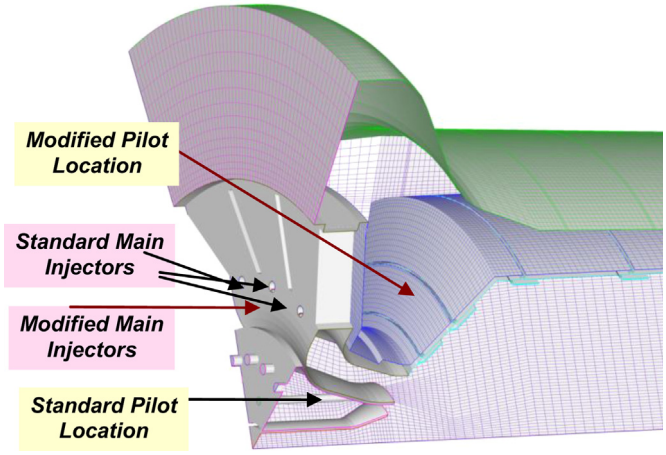

Fig. 9. Standard and modified injector locations.

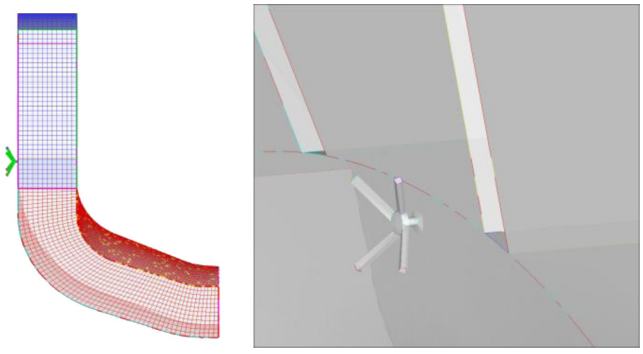

Fig. 10. Detailed sketch of the modified liquid fuel injector.

- The turbulent flow solution founds on the realizable $k-\varepsilon$ model;
- The reacting, multiphase flow simulation includes the prediction of the droplet atomization process with the TAB model.
- The finite rate – eddy dissipation concept [26] is adopted for the fuel oxidation. The kinetic mechanisms is based on the following scheme:

$$
\begin{aligned}
&1)\ C_{12}H_{23} + 17.75O_2 \Rightarrow 12CO_2 + 11.5H_2O \\
&R_1 = 2.587{*}10^9 [C_{12}H_{23}]^{0.25} [O_2]^{1.5} e^{-\frac{1.256{*}10^8}{T}} \\
&2)\ C_2H_5OH + 3O_2 \Rightarrow 2CO_2 + 3H_2O \\
&R_2 = 8.435{*}10^9 [C_2H_5OH]^{0.15} [O_2]^{1.6} e^{-\frac{1.256{*}10^8}{T}} \\
&3)\ CO_2 \Rightarrow CO + 1/2O_2 \\
&R_3 = 5{*}10^8 [CO_2][O_2]^{0.25} e^{-\frac{1.7{*}10^8}{T}} \\
&4)\ CO + \frac{1}{2}O_2 \Rightarrow CO_2 \\
&R_4 = 2.239{*}10^{12} [CO][O_2]^{0.25} e^{-\frac{1.674{*}10^8}{T}}
\end{aligned}
\qquad (2)
$$

- The nitric oxide prediction includes the computation of both thermal and prompt NO.
- The inlet and boundary conditions (i.e., mass flow rates, and temperatures), together with the combustor outlet pressure, are derived from a preliminary thermodynamic analysis of the system.

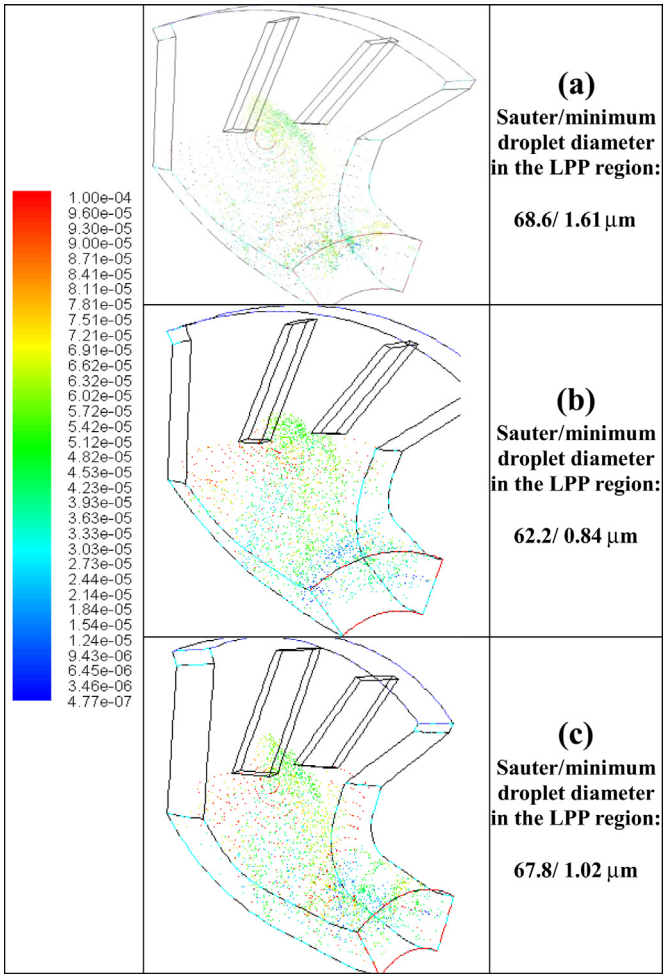

Fig. 12. Droplet diameter [m] distribution with the hollow cone model.

- An initial droplet diameter of 50 μm was assumed for both main and pilot injection, with a velocity of the liquid phase of 30 m/s.

Prior to the examination of the bio-ethanol based processes, the effect of the modified injector type and location for the main LPP line was investigated. Fig. 14 displays the liquid jet pattern together with the droplet diameter distribution from the standard and the modified injection system. Although the replacement of

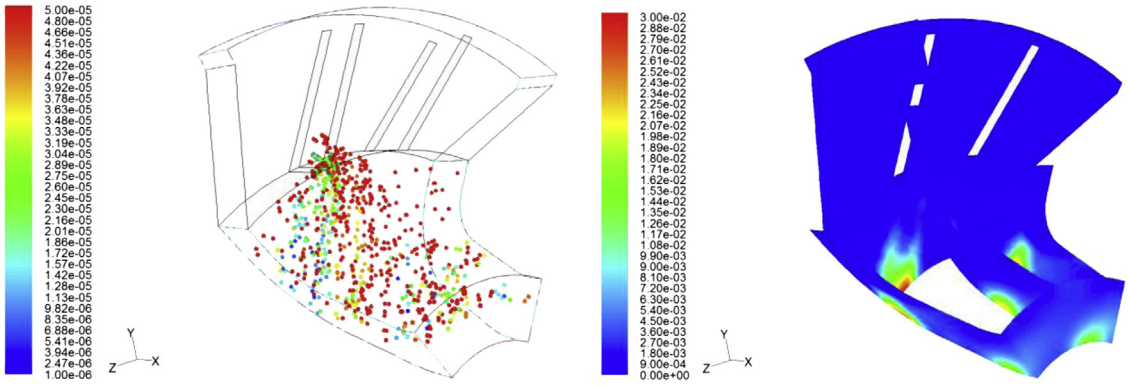

Fig. 11. Droplet diameter [m] and fuel vapour distribution with the swirling fuel injector.

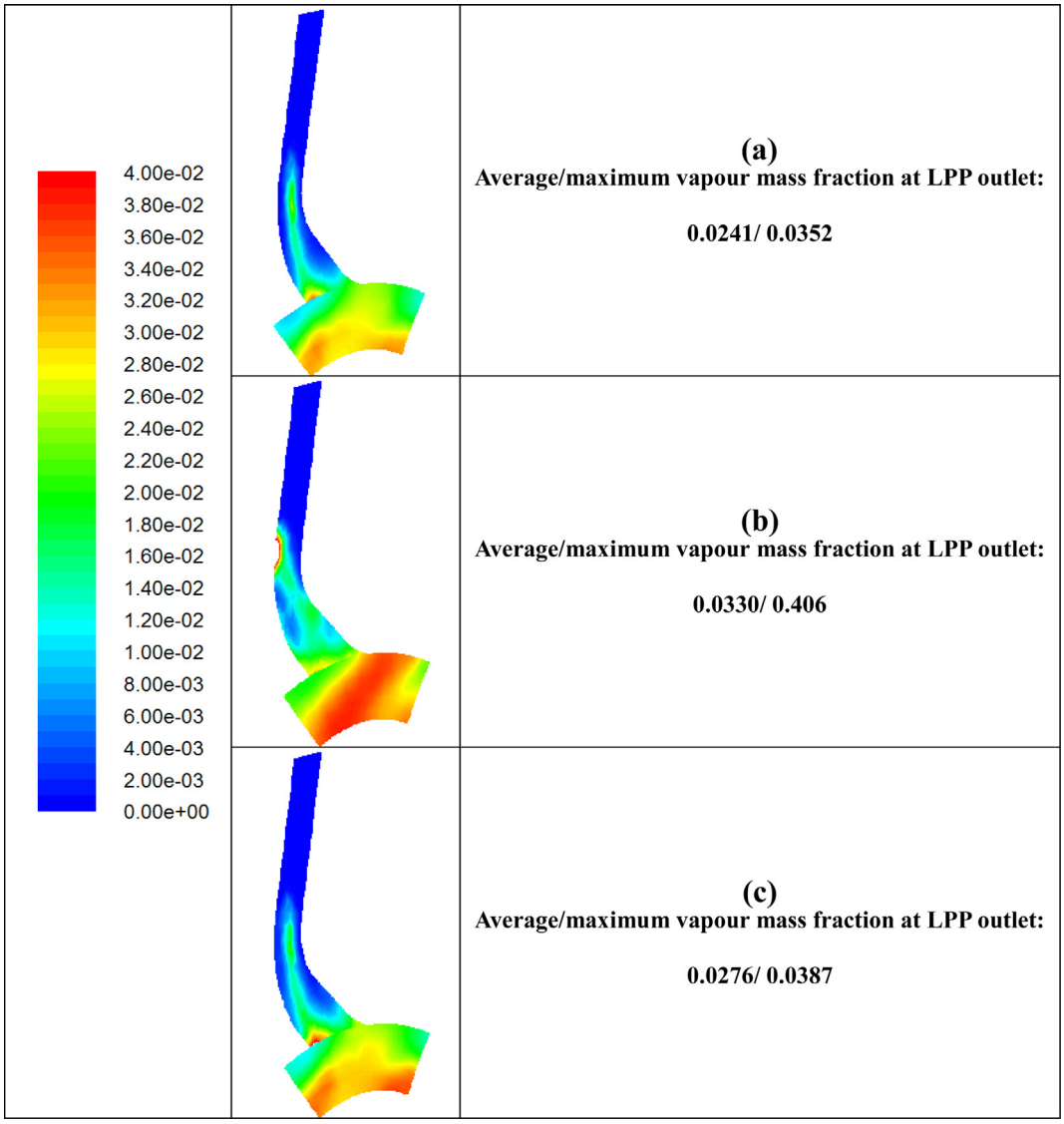

Fig. 13. Fuel vapour distribution with the hollow cone model.

12 radial injectors with a single swirling injector (for each 60° sector) represents an affordable technical solution, the droplet distribution appears to be less uniform than in the standard injection case. The atomization itself seems to be slower and the fuel – air mixing is not homogeneous, as already detectable in Fig. 11.

Nevertheless, the comparison of the results of the kerosene combustion with the two different injection systems (Table 5) provides encouraging indications in terms of combustion efficiency, since the firing temperatures are quite similar and the unburned and CO fractions are negligible in both cases. On the other hand, the reduced homogeneity in the reacting mixture results in increased temperature peaks and, as a consequence, in higher nitric monoxide concentration. Actually, both the average and the maximum NO formation rates (Table 6) are higher when the single swirling injector is considered.

The existence of a more extended region with peak temperature levels is confirmed by the contours in Fig. 15, in the case of the modified main injector. This situation does not exert a significant influence on the temperature distribution at the combustor outlet (Fig. 16) but it strongly affects the nitric oxide formation, whose maximum concentration is attained in the highest temperature regions (Fig. 17). The related distributions in the outlet sections (Fig. 18) indicate a noticeable emission increase when the single swirling injector is operated. Therefore, the combined adoption of the modified pilot injector location is strictly suggested, in order to attenuate the pollutant formation rates.

The effect of the variation in the pilot jet stream (Fig. 14) has been studied in the case of the bio-ethanol fuelling. The results in Tables 5 and 6 underline the positive influence exerted by the modified injector location: a significant NO abatement takes place as a consequence of the formation rates whose average and maximum values are reduced by an order of magnitude with respect to the case with the standard pilot location. Such reduction reductions derive from the noticeable decrease in the temperature peak. On the other hand, no relevant change is observed in the combustion effectiveness, if looking at the unburned and CO mass fractions. In Fig. 19, the contours of the fuel vapour mass fraction confirm that the reactant distribution undergoes strong variations as a consequence of the shifted pilot location. This

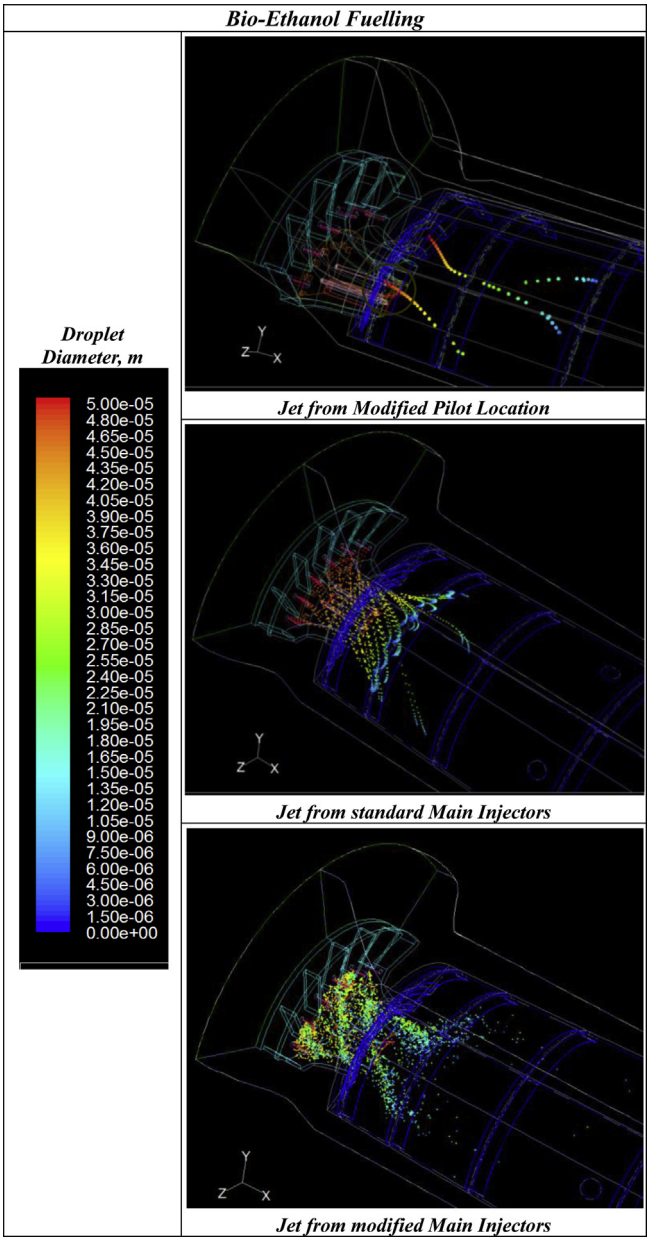

Fig. 14. Droplet distribution in the primary region of the combustor.

results in a reduced flame intensity, like demonstrated by the temperature contours in Fig. 20. Examining this figure together with the results in Table 5 leads to the following encouraging conclusions:

Table 5
Volume-averaged and outlet properties from CFD based simulations.

Fuel/pilot	Volume		Outlet			
	$[\overline{O}_2]$%, mol	T_{max}, K	$\overline{T}_{ex}$, K	[NO] p.p.m.	[CO] p.p.m.	[UHC] p.p.m.
Kerosene/standard	18.36	2730	1238	209	27.2	1.1×10^{-4}
Kerosene/new main	18.06	2791	1264	382	32.8	7.8×10^{-5}
Bio-ethanol/new main	18.18	2698	1236	225	34	2.0×10^{-4}
Bio-ethanol/new main & pilot	18.29	2277	1243	80	30	3.6×10^{-4}

Table 6
Volume-averaged and maximum of reaction and nitric oxides rates.

Fuel/pilot	Value	Overall NO rate, kmole/(m^{3}s)	Fuel oxidation rate, kmole/(m^{3}s)
Kerosene/standard	Average	5.08×10^{-4}	4.99×10^{-3}
	Maximum	4.02×10^{-1}	2.274
Kerosene/new main	Average	1.03×10^{-3}	4.98×10^{-3}
	Maximum	6.22×10^{-1}	1.578
Bio-ethanol/new main	Average	4.54×10^{-5}	2.75×10^{-2}
	Maximum	4.39×10^{-2}	24.11
Bio-ethanol/new main & pilot	Average	6.25×10^{-7}	2.79×10^{-2}
	Maximum	2.79×10^{-3}	7.49

- The flameless regime may be considered as approached, since a much smoother temperature profile is obtained in the primary region, if comparing the situations with the standard and modified location of the pilot injector. This confirms that the primary process is activated within an oxygen-poor, intern-rich region.
- As a further proof, the temperature peak are greater than the standard adiabatic flame temperature in all cases, because the combustion process starts from temperatures above 900 K; only with the modified pilot location, much lower peaks are attained.

4.2. Gaseous fuel supply

The CFD simulations were also addressed to the analysis of the combustion of gaseous fuels, i.e., methane and biogas. The computations aim at the comparison of the response of a conventional fuel with the one of a gaseous biofuel [27]. An intermediate step is represented by the injection of biogas to the premixing line and of

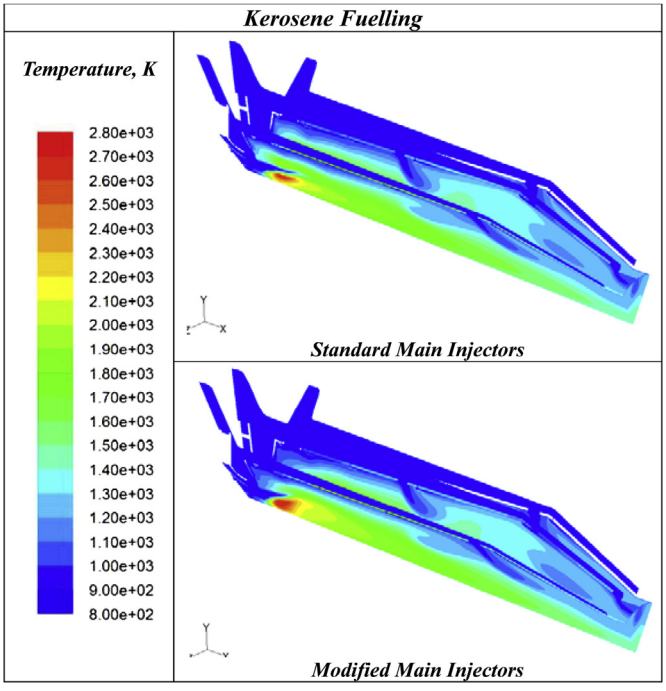

Fig. 15. Temperature distributions for different main injections.

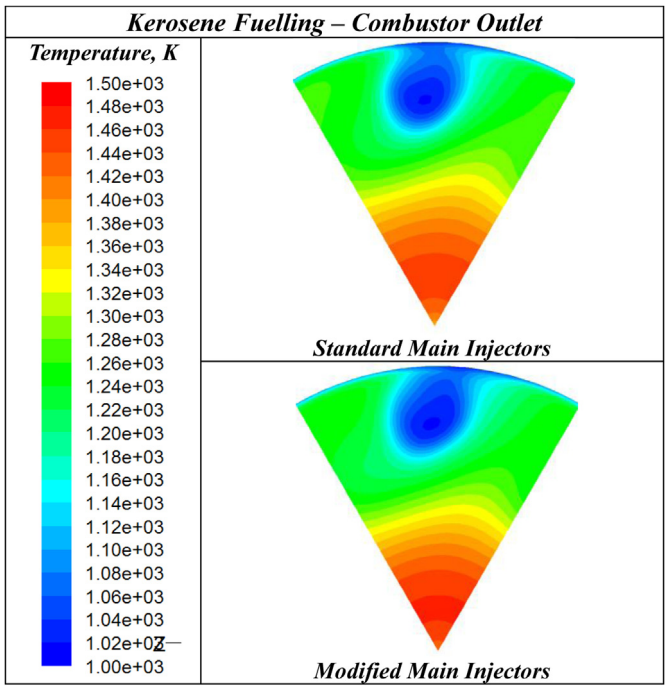

Fig. 16. Temperature distributions for different main injections.

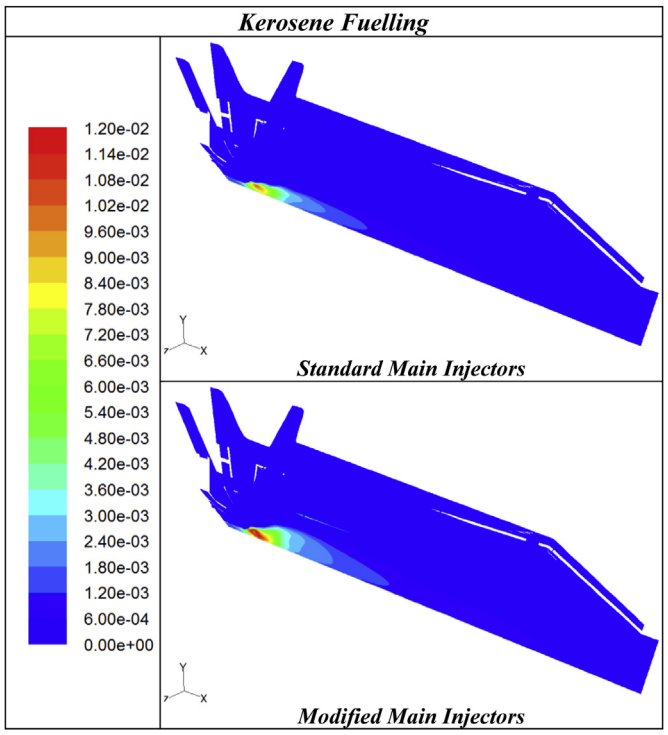

Fig. 17. NO mass fraction distributions for different main injections.

methane to the pilot line. Such a solution would be helpful to a faster ignition and it would be also needed during the start-up phases. Both the main and the pilot injection systems are considered to be the standard ones in Figs. 8 and 9.

The computational case setup is similar to the one described for the liquid fuels and refers to the data in Tables 1 and 2. Regarding to the oxidation mechanism the 8-step scheme proposed by Novosselov and Malte [28] was selected. It should be remarked that the chain of kinetic Eq. (3) include different mechanisms of thermal and prompt NO: therefore, the reactions (4)–(8) are only apparently the same, but they are summarizing a variety of phenomenologies of nitric oxide formation. In addition, such equations are temperature and pressure sensitive, so that a feasible employment is expect in a wide range of operating conditions.

$$
\begin{aligned}
&1)\ CH_4 + 3/2O_2 \Rightarrow CO + 2H_2O\\
&R_1 = 10^{13.354-0.004628P}[CH_4]^{1.3-0.01148P}[O_2]^{0.01426}[CO]^{0.1987}e^{-\frac{21932+269.4P}{T}}\\
&2)\ CO + 1/2O_2 \Rightarrow CO_2\\
&R_2 = 10^{14.338-0.1091P}[CO]^{1.359-0.0109P}[H_2O]^{0.0912+0.0909P}[O_2]^{0.891+0.0127P}e^{-\frac{22398+75.1P}{T}}\\
&3)\ CO_2 \Rightarrow CO + 1/2O_2\\
&R_3 = 10^{15.8144+0.07163P}[CO_2]e^{-\frac{64925.8-334.31P}{T}}\\
&4)\ N_2 + O_2 \Rightarrow 2NO\\
&R_4 = 10^{14.122+0.0376P}[O_2]^{1.1805+0.0344P}[CO]^{0.8888-0.0006P}e^{-\frac{46748+126.6P}{T}}\\
&5)\ N_2 + O_2 \Rightarrow 2NO\\
&R_5 = 10^{29.8327-4.7822\ \log(P)}[O_2]^{2.4613}[CO]^{2.7911-0.04880P}e^{-\frac{61265+704.7P}{T}}\\
&6)\ N_2 + O_2 \Rightarrow 2NO\\
&R_6 = 10^{14.592}[N_2][H_2O]^{0.5}[O_2]^{0.25}T^{-0.7}e^{-\frac{69158}{T}}\\
&7)\ N_2 + O_2 \Rightarrow 2NO\\
&R_7 = 10^{10.317}[N_2][O_2]e^{-\frac{52861}{T}}\\
&8)\ N_2 + O_2 \Rightarrow 2NO\\
&R_8 = 10^{14.967}[N_2][O_2]^{0.5}T^{-0.5}e^{-\frac{68899}{T}}
\end{aligned}
\tag{3}
$$

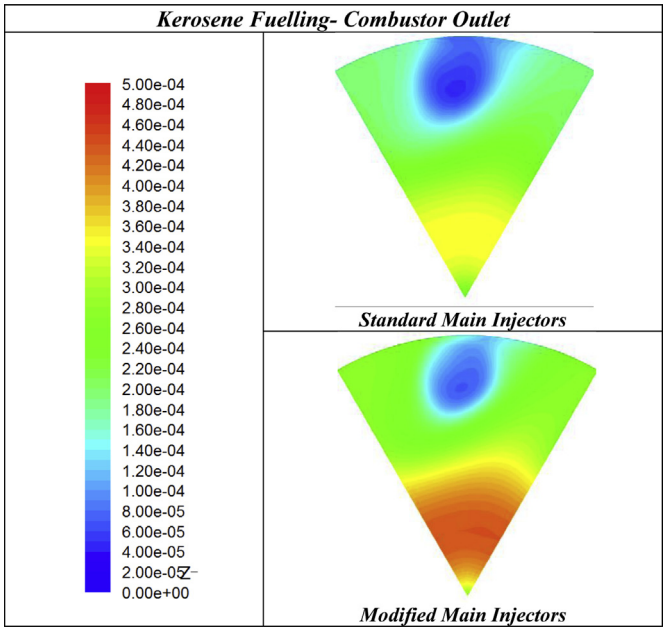

Fig. 18. NO mass fraction distributions for different main injections.

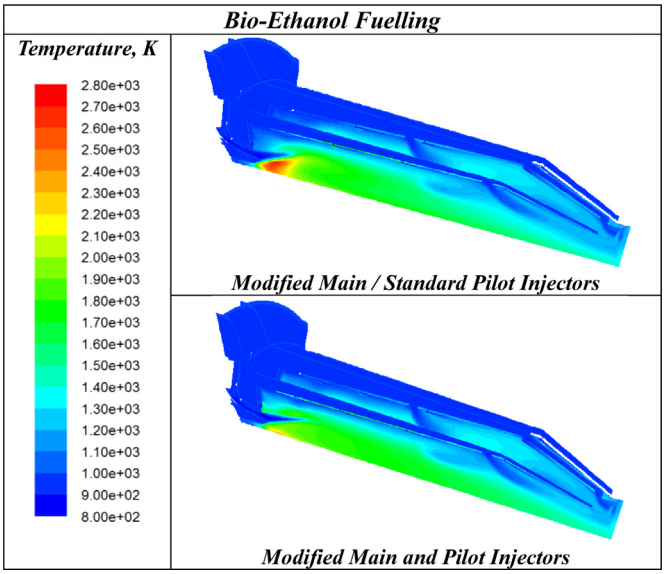

Fig. 20. Temperature distributions for different pilot locations.

The result overview in Tables 7 and 8 put into evidence that a satisfactory combustion completion occurs also when fuelling the micro gas turbine with biogas from both the injection systems. The "methane from pilot" solution leads to results fairly similar to those with methane fuelling, also in terms of NO emission and formation rates. Therefore, this option may be considered only under particular conditions like start-up or transient operations. As expected, the CO_2 contents in the biogas exerts a positive influence on the reduction of the NO formation rates, while a non-negligible increase in carbon monoxide can be observed.

In accordance with the preliminary indications provided by the thermodynamic – thermo-kinetic analysis (Figs. 2 and 3) a further benefit in terms of NO reduction could be obtained by activating the external EGR options. It is worth-noting that the biogas fuelling requires to this purpose an EGR rate much lower than the one need for natural gas fuelling, so preserving an acceptable level of thermal efficiency. Therefore, according to diagrams in Figs. 2 and 3, an EGR rate of 40% appears to be sufficient for a satisfactory control of the nitric oxide formation. The results in the last rows of Tables 7 and 8 confirm such an expectation: actually, a significant cut-off of both temperature peak and NO formation rates can be observed, while the fuel oxidation rate is not affected. So, the decrease in NO contents is not counterbalanced by increases in CO and UHC. Like in the liquid fuel case, temperature peaks higher than the standard adiabatic flame ones can be observed, because of the relevant air temperature at combustor inlet; only the 40% EGR case induces a significant attenuation of such phenomenon. It should be considered that a reduced EGR rate has been chosen, in order to find the best compromise between pollutant reduction and performance

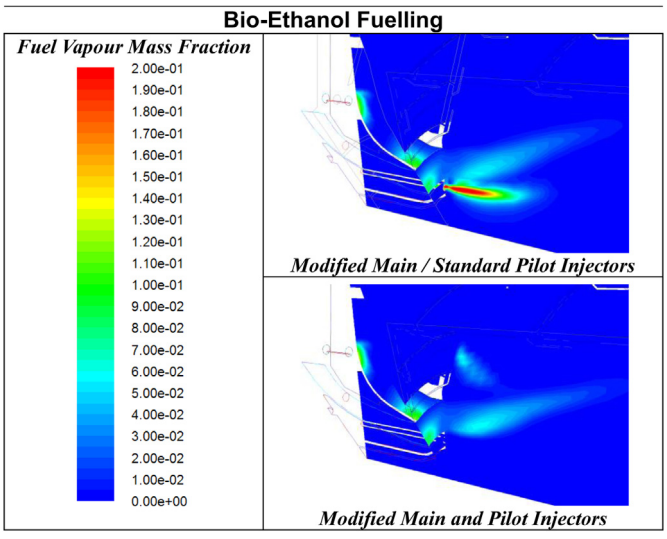

Fig. 19. Fuel vapour distributions for different pilot locations.

Table 7
Volume-averaged and outlet properties from CFD based simulations.

Fuel/pilot	Volume		Outlet			
	$[\overline{O}_2]$%, mol	T_{max} K	$\overline{T}_{ex}$ K	[NO] p.p.m.	[CO] p.p.m.	[UHC] p.p.m.
Methane	18.52	2637	1227	125	586	2.95
Biogas/methane from pilot	18.51	2638	1219	125	856	5.74
Biogas	18.45	2559	1223	112	865	5.96
Biogas 40% EGR	16.03	2439	1219	28	841	5.85

Table 8
Volume-averaged and maximum of reaction and nitric oxides rates.

Fuel/pilot	Value	Thermal + prompt NO rate, kmole/(m^{3}s)	Fuel oxidation rate, kmole/(m^{3}s)
Methane	Average	2.26×10^{-4}	4.26×10^{-2}
	Maximum	1.72×10^{-1}	101.5
Biogas/methane from pilot	Average	2.26×10^{-4}	4.25×10^{-2}
	Maximum	1.41×10^{-1}	103.2
Biogas	Average	1.43×10^{-4}	4.24×10^{-2}
	Maximum	5.10×10^{-2}	53.11
Biogas 40% EGR	Average	2.79×10^{-5}	4.25×10^{-2}
	Maximum	9.60×10^{-3}	68.55

preservation. Higher EGR levels would induce, of course, a closer approach to the flameless regime [1].

In Fig. 21, some differences can be observed when adopting the mixed solution (i.e., methane injection from pilot) or the full biogas supply. The latter induces a lower methane concentration downstream of the pilot and this gives reason of the result in Tables 7 and 8, in terms of reduction in temperature peaks and NO formation rates. A more relevant effect on these parameters is exerted by the EGR activation, like confirmed by the temperature distributions in Fig. 22.

A final remark should be addressed to the levels of nitric monoxides as predicted by the CFD simulations (Tables 5 and 7). Actually, such levels appear to be considerably higher than those estimated by the thermo-kinetic model (Tables 2 and 4). This is probably due to the need of an appropriate calibration of the models implemented in the reacting flow solver, but it also depends on a number of factors, say:

- The CFD solver provides a more accurate estimation of the local temperature peaks and of the fuel/air ratios in the different combustor regions;
- The models for the NO mechanism do not incorporate the backward reactions for the nitric oxide reduction.

Nevertheless, the differences between the several computational cases are consistent with the preliminary predictions. For example, the emissions from liquid fuels are higher than those from gaseous fuels and both the external and internal EGR options operate correctly, with a relevant reduction (at least by one order of magnitude) of the NO formation rates. Under these aspects, the results from the CFD analysis can be considered an helpful tool for evaluating the effectiveness of the several solutions that have been examined.

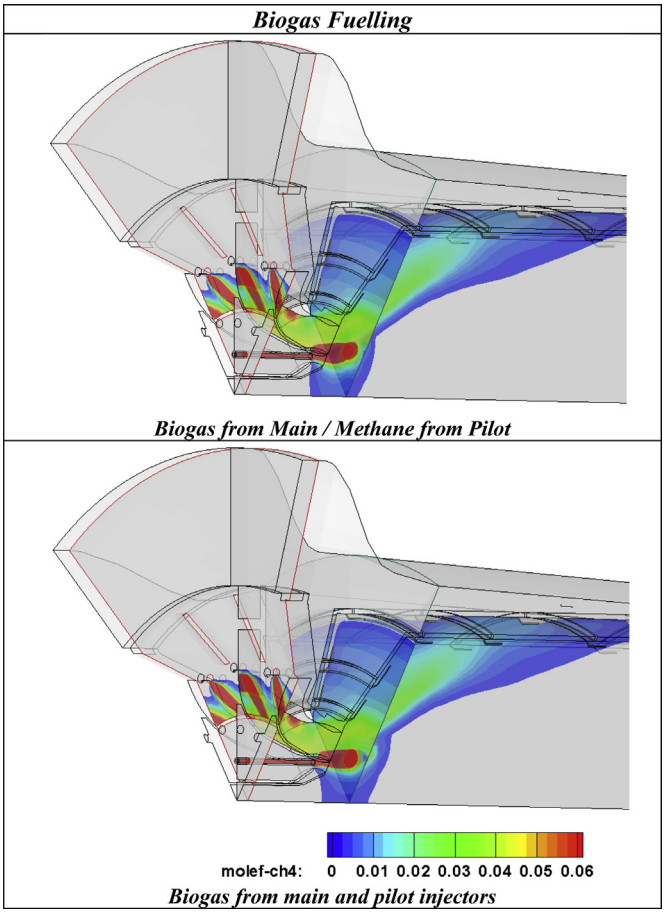

Fig. 21. Methane distribution for different fuel supplies.

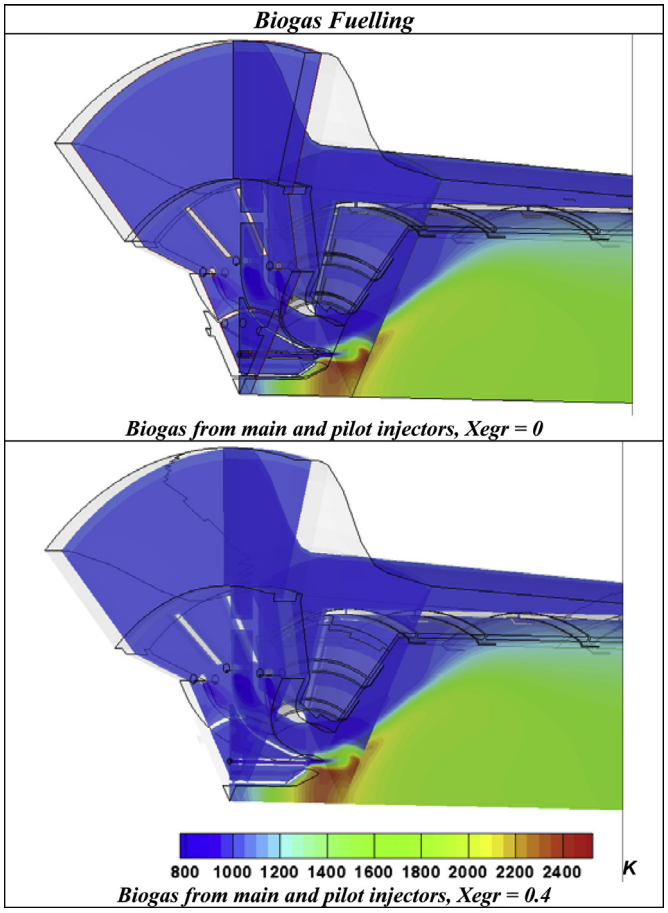

Fig. 22. The EGR effect on the temperature distributions.

5. Conclusion

This paper has discussed a number of solutions for an efficient employment of liquid and gaseous bio-fuels in a typical lean-premixed combustor of a micro-gas turbine. The results from the CFD analysis indicate a fairly satisfactory response of these fuels from the energetic and environmental point of view. Actually, both the bio-ethanol and the biogas fuelling exhibit a suitable behaviour in terms of combustion completion. In addition, reduced emission levels at baseline operation can be observed if comparing the pollutant level induced by the bio-fuels with the one from conventional fossil resources like kerosene or natural gas.

The above information, besides encouraging the use of fuels from renewable sources, suggests the need for further improvements in terms of control of nitric oxide emissions. In this sense some options, which have been already experienced by the authors in their previous works, have confirmed an acceptable effectiveness. In particular, the modified location of the pilot injector allows approaching a nearly flameless combustion regime. As an alternate method, the activation of the external *EGR* circuit leads to decreased NO emissions, without introducing penalties in combustion efficiency. It is worth-noting that accessing such an option

when supplying the micro-turbine with a biogas requires a reduced EGR ratio, so preserving an acceptable level of thermal efficiency.

Finally, the liquid bio-fuel combustion has been examined with a modified swirling injector type and location within the LPP line. This solution allows the original injectors for fuel gas supply to be maintained. In this way, an easier dual-fuel operation can be considered for a more efficient combustion under particular conditions that are usually induced by part-load or start-up operation.

Acknowledgements

To *Ansaldo Ricerche S.p.A.* for providing data on the MGT parameters and combustor configuration. The CFD calculations are performed by the *ANSYS-Fluent flow solver.*

References

[1] M.C. Cameretti, F. Reale, R. Tuccillo, Cycle Optimization and combustion analysis in a low-NOx micro-gas turbine, ASME J. Gas Turbines Power 129 (2007) 994–1003, http://dx.doi.org/10.1115/1.2718232.
[2] M.C. Cameretti, F. Reale, R. Tuccillo, NOx Suppression from a Micro-gas Turbine Approaching the Mild-combustion Regime (2007). ASME Paper no. GT2007-27091.
[3] M.C. Cameretti, R. Piazzesi, F. Reale, R. Tuccillo, Combustion simulation of an EGR operated micro-gas turbine, ASME J. Gas Turbines Power 131 (2009) 051701-1–051701-10, http://dx.doi.org/10.1115/1.3078193.
[4] M.C. Cameretti, R. Piazzesi, F. Reale, R. Tuccillo, CFD Analysis of the Flameless Combustion in a Micro-gas Turbine (2009). ASME paper GT2009-58750.
[5] M.C. Cameretti, R. Piazzesi, F. Reale, R. Tuccillo, Comparison of External and Internal EGR Concepts for Low Emission Micro Gas Turbines (2010). ASME paper GT2010-22413amprdquosemicolon.
[6] M.C. Cameretti, R. Piazzesi, F. Reale, R. Tuccillo, Liquid Bio-fuels in an EGR Equipped Micro Gas Turbine (2011). ASME paper GT2011-46341.
[7] T. Panne, A. Widenhorn, M. Aigner, Comparison of Combustion Models and Reaction Mechanisms for FLOX® Combustion (2009). ASME paper GT2009-59075.
[8] B. Danon, E.-S. Cho, W. de Jong, D.J.E.M. Roekaerts, Numerical investigation of burner positioning effects in a multi-burner flameless combustion furnace, Appl. Therm. Eng. 31 (17–18) (December 2011) 3885–3896.
[9] Y. Levy, V. Sherbaum, G.A. Rao, Preliminary Analysis of a New Methodology for Flameless Combustion in Gas Turbine Combustors (2007). ASME paper GT2007-27766.
[10] G. Li, E.J. Gutmark, N. Overman, Michael Cornwell, Experimental Study of a Flameless Gas Turbine Combustor (2006). ASME paper GT2006-91051.
[11] P. Dagaut, T.L. Cong, Kinetics of Natural Gas, Natural Gas/Syngas Mixtures Oxidation and Effect of Burnt Gas Recirculation: Experimental and Detailed Modeling (2007). ASME paper GT2007-27146.
[12] Y. Levy, V. Sherbaum, V. Erenburg, The Role of the Recirculating Gases at the Mild Combustion Regime Formation (2007). ASME paper GT2007-27369.
[13] Y. Levy, V. Sherbaum, V. Erenburg, Effect of the recirculation gases on the mild combustion regime, Int. J. Turbo Jet-Engines 26 (2009) 9–18.
[14] M.C. Cameretti, R. Piazzesi, R. Tuccillo, Fuelling an EGR Equipped Micro Gas Turbine with Bio-fuels (2012). ASME paper GT2012-68720.
[15] A. Cavaliere, M. de Joannon, Mild combustion, Prog. Energy Combust. Sci. 30 (4) (2004), http://dx.doi.org/10.1016/j.pecs.2004.02.003. (Elsevier).
[16] G. Lastella, et al., Anaerobic digestion of semi-solid organic waste: biogas production and its purification, Energy Convers. Manage. 43 (2002) 63–75. (Elsevier).
[17] K..K. Gupta, A. Rehman, R.M. Sarviya, Bio-fuels for the gas turbine: a review, Renew. Sustain. Energy Rev. (2010) 2946–2955, http://dx.doi.org/10.1016/j.rser.2010.07.025. (Elsevier).
[18] M. Prussi, D. Chiaramonti, G. Riccio, F. Martelli, L. Pari, Straight vegetable oil use in micro-gas turbines: system adaptation and testing, Appl. Energy 89 (2012) 287–295, http://dx.doi.org/10.1016/j.apenergy.2011.07.031. (Elsevier).
[19] J. Barata, Modelling of biofuel droplets dispersion and evaporation, Renew. Energy 33 (2008) 769–779, http://dx.doi.org/10.1016/j.renene.2007.04.019.
[20] A. Amoresano, M. Cameretti, R. Tuccillo, Combined Experimental – Numerical Approach for the Fuel Jet Study in a LPP Combustor (2011). ASME paper GT2011-46339.
[21] Hu Li, M. Altaher, G.E. Andrews, Evaluation of Combustion and Emissions Using Biodiesel and Blends with Kerosene in a Low Nox Gas Turbine Combustor (2010). ASME paper GT2010-22182.
[22] P.A. Glaude, et al., Ethanol as an Alternative Fuel in Gas Turbines: Combustion and Oxidation Kinetics (2010). ASME paper GT2010-22338.
[23] Zehra Habib, Ramkumar Parthasarathy, Subramanyam Gollahalli, Performance and emission characteristics of biofuel in a small-scale gas turbine engine, Appl. Energy 87 (2010) 1701–1709, http://dx.doi.org/10.1016/j.apenergy.2009.10.024. (Elsevier).
[24] Pierre-Alexandre Glaude, René Fournet, Roda Bounaceur, Michel Molière, Adiabatic flame temperature from biofuels and fossil fuels and derived effect on NOx emissions, Fuel Process. Technol. 91 (2010) 229–235, http://dx.doi.org/10.1016/j.fuproc.2009.10.002. (Elsevier).
[25] M. Moliere, et al., Gas Turbines in Alternative Fuel Applications: Bio-ethanol Field Test (2009). ASME paper GT2009-59047.
[26] C. Russo, J. Parente, G. Mori, V. Anissimov, Micro Gas Turbine Combustor Emissions Evaluation Using the Chemical Reactor Modelling Approach (2007). ASME paper GT2007-27687.
[27] M. Cadorin, M. Pinelli, A. Vaccari, R. Calabria, F. Chiariello, P. Massoli, E. Bianchi, Analysis of a micro gas turbine fed by natural gas and synthesis gas: MGT test bench and combustor CFD analysis, ASME J. Gas Turbines Power 134 (2012) 071401–071411, http://dx.doi.org/10.1115/1.4005977.
[28] I.V. Novosselov, P.C. Malte, Development and Application of an Eight-step Global Mechanism for CFD and CRN Simulations of Lean-premixed Combustors (2007). ASME paper GT2007-27990.